Impact of Small-Scale Rainfall Variability on Larger-Scale Spatial Organization of Land–Atmosphere Fluxes

DEBORAH K. NYKANEN* AND EFI FOUFOULA-GEORGIOU

St. Anthony Falls Laboratory, Department of Civil Engineering, University of Minnesota, Minneapolis, Minnesota

WILLIAM M. LAPENTA

NASA MSFC Global Hydrology and Climate Center, Huntsville, Alabama

(Manuscript received 26 May 2000, in final form 6 December 2000)

ABSTRACT

A coupled modeling framework is used in this study to investigate the effect of subgrid-scale rainfall variability on the spatial structure of the evolving storm and on other surface variables and water and energy fluxes. The Fifth-Generation Pennsylvania State University–National Center for Atmospheric Research Mesoscale Model coupled with the Biosphere–Atmosphere Transfer Scheme is combined with a dynamical/statistical scheme for statistically downscaling rainfall. Model simulations with and without including subgrid-scale rainfall variability are compared at the grid scale to quantify the propagation of small-scale rainfall heterogeneities through the nonlinear land–atmosphere system. It was found that including subgrid-scale rainfall variability (here on the order of 3 km) affects the spatial organization of the storm system itself, surface temperature, soil moisture, and sensible and latent heat fluxes. These effects were found to occur at spatial scales much larger than the scale at which rainfall variability was prescribed, illustrating the pronounced nonlinear spatial dynamics of the land–atmosphere system and its important role on hydrometeorological predictions.

1. Introduction

Understanding the space–time variability of rainfall at a range of spatial and temporal scales and improving its representation in coupled atmospheric–hydrologic models is of critical importance in advancing our ability to predict variations in weather and climate. This study investigates to what degree the small-scale ($\leq$10–20 km) variability of rainfall is important in modulating the spatial organization of water and energy fluxes in the coupled land–atmosphere system.

Observed rainfall has been shown to have significant variability at scales much smaller than the typical grid sizes of mesoscale or global circulation models, down to the scale of a few meters (e.g., Schertzer and Lovejoy 1987; Gupta and Waymire 1990; Perica and Foufoula-Georgiou 1996a; Harris et al. 1996). Previous studies have documented the importance of small-scale rainfall variability on the simulated runoff from a basin using rainfall–runoff models for which rainfall was prescribed offline and was not coupled to the land surface (e.g., see Kouwen and Garland 1989; Krajewski et al. 1991; Ogden and Julien 1993, 1994; Michaud and Sorooshian 1994; Obled et al. 1994; Faures et al. 1995; Winchell et al. 1998). It is known, however, that the land surface and the atmosphere interact and influence each other through nonlinear feedbacks and act as a coupled system. Thus, a more accurate evaluation of the effects of subgrid-scale rainfall variability is expected to result when a coupled land–atmosphere model is used.

The impact of ignoring the subgrid-scale rainfall variability (i.e., second- and higher-order moments) and the propagation of this variability via the nonlinear equations of the coupled land–atmosphere system can result in significant biases of the predicted variables at scales larger than the scale of the prescribed rainfall variability. This point is schematically illustrated in Fig. 1 which considers the nonlinear evolution of a variable X at two different scales: a small scale (top) and a larger scale (bottom). This schematic demonstrates that, even if the scale of interest is large, predicting the evolution of $\overline{X}$ at a later time [i.e., $\overline{X} \rightarrow F(\overline{X})$ where F is a nonlinear operator] is not the same as predicting that variable at

* Current affiliation: Department of Civil and Environmental Engineering, Michigan Technological University, Houghton, Michigan.

Corresponding author address: Deborah K. Nykanen, Dept. of Civil and Environmental Engineering, Michigan Technological University, 1400 Townsend Dr., Houghton, MI 49931.
E-mail: dnykanen@mtu.edu

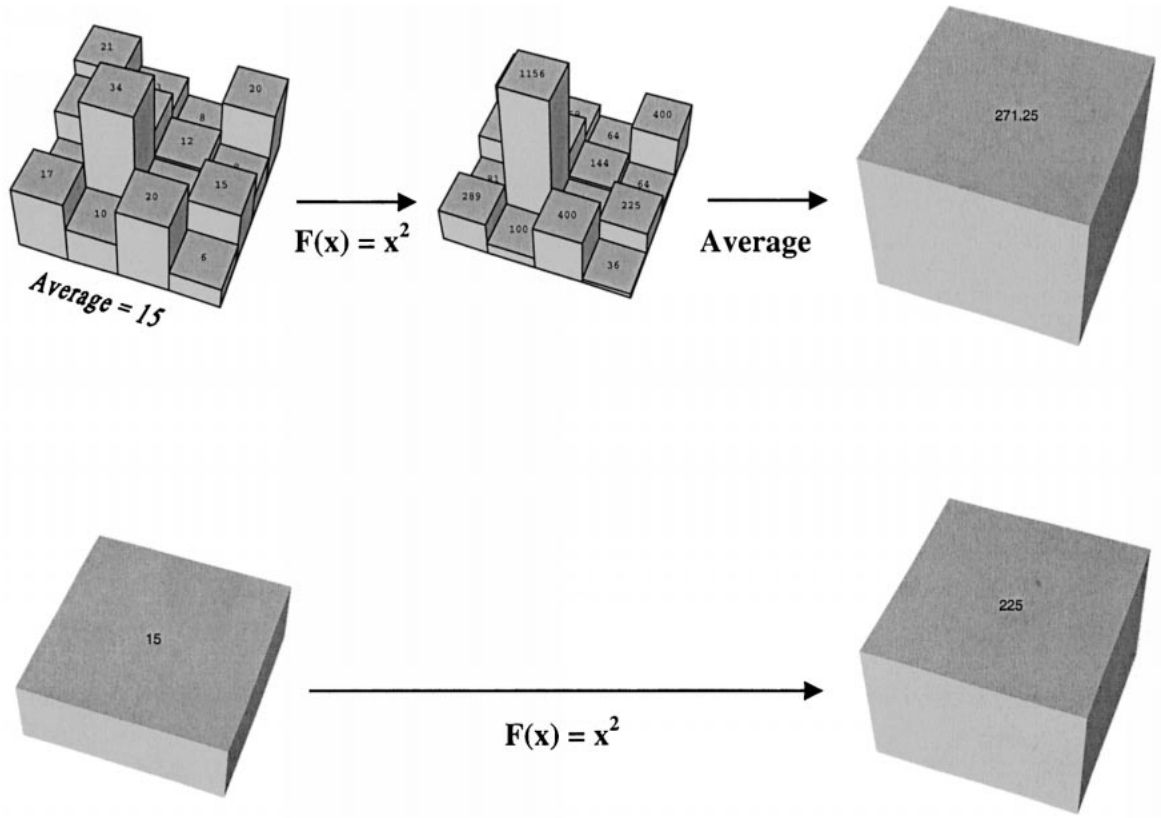

FIG. 1. Nonlinear evolution of a variable X at two different scales. Depending on the temporal gradient of the nonlinear operator F and the magnitude of the subgrid-scale variance of X, the prediction at the larger scale $F(\overline{X})$ (bottom) can be very different from the average of the small-scale predictions $\overline{F(X)}$ (top).

smaller scales and computing an average of these predictions, that is, $\overline{F(X)} = \frac{1}{4}[F(X_1) + F(X_2) + F(X_3) + F(X_4)] \neq F(\overline{X})$. The approach on top has explicitly considered the subgrid-scale variability of the variable, and $\overline{F(X)}$ includes this effect; the approach at the bottom has ignored the subgrid-scale variability. Depending on the temporal gradient of the operator F and the magnitude of the subgrid-scale variance, $F(\overline{X})$ can be very different from $\overline{F(X)}$.

A first step toward evaluating the effects of subgrid-scale rainfall variability in the coupled land–atmosphere system was done by Zhang and Foufoula-Georgiou (1997). That study used The Fifth-Generation Pennsylvania State University–National Center for Atmospheric Research Mesoscale Model (MM5) with its Blackadar planetary boundary layer scheme to assess the effects of subgrid-scale rainfall variability on the surface temperature distribution and further development of the storm system itself. The results indicated significant effects and pointed out the need for more rigorous quantitative assessment, especially using more accurate representation of the land–atmosphere exchanges. The current study aims toward this direction. It uses the MM5 model coupled with the Biosphere–Atmosphere Transfer Scheme (BATS) to capture better the nonlinear feedbacks between the highly variable rainfall and the surface/subsurface response of a basin. The scope is to investigate how subgrid-scale variability of rainfall affects the prediction of the evolving storm, surface variables, and water and energy fluxes when the coupling of the land and atmosphere is properly acknowledged.

This paper is structured as follows. In section 2, the MM5–BATS model is briefly described together with the statistical rainfall downscaling scheme and its two-way coupling with MM5–BATS. Section 3 presents the details of the numerical experiment. The research methodology used in this study to allow the subgrid-scale rainfall variability to propagate through the coupled MM5–BATS land–atmosphere system is described in section 4. This section also presents verification that the variability added to the rainfall at the subgrid scale is reasonable. The results of the numerical experiment are discussed in section 5, and conclusions are presented in section 6.

2. Model description

a. MM5–BATS coupled model

The MM5 mesoscale model coupled with the BATS land surface scheme was used in this study to simulate

atmospheric and surface conditions over a 48-h period. The MM5 modeling system contains state-of-the-art features such as multiple-nest capability, hydrostatic and nonhydrostatic dynamics, four-dimensional data assimilation, vertical terrain-following sigma coordinate, many physics options, as well as multitasking capabilities on shared- and distributed-memory machines (Grell et al. 1995; Michalakes 1998).

The coupling of BATS with MM5 provides a more detailed land–atmosphere interaction scheme than is otherwise available with MM5 alone (Lakhtakia and Warner 1994). Dickinson et al. (1993) gives a detailed description of the physical processes and parameterizations used in BATS. One of the main advantages of BATS over the simple force–restore slab model typically used in MM5 is that it contains a more sophisticated biophysically based representation of vegetation and its effects on energy and water fluxes. In addition, BATS has more realistic soil hydrologic processes than the standard slab-type model. BATS has three soil layers with infiltration, percolation, vegetation root structure, and heat exchange between the layers. It has the capability of plants to intercept and to evaporate part of the precipitable water and can have coexistence of bare-soil and vegetated subareas within a grid box. BATS also has time-dependent surface characteristics and time-dependent soil hydrologic behavior. For example, the moisture availability changes throughout the simulation based on rainfall and evaporative processes. A detailed description of the differences between BATS and the slab-type land surface schemes in MM5 and the corresponding effects of these differences can be found in Lakhtakia and Warner (1994).

b. Subgrid-scale rainfall variability and downscaling

Based on statistical analysis of numerous mesoscale convective storms, Perica and Foufoula-Georgiou (1996a) found that standardized spatial rainfall fluctuations ($\xi_L = X'_L/\overline{X}_L$, where X'_L is the difference in rainfall intensities at adjacent pixels of scale L in the longitudinal, latitudinal, and diagonal directions and $\overline{X}_L$ is the average rainfall intensity at that same scale) exhibited Gaussianity and simple scaling (see also Kumar and Foufoula-Georgiou 1993a,b), implying that

$$\frac{\sigma_{\xi,L_1}}{\sigma_{\xi,L_2}} = \left(\frac{L_1}{L_2}\right)^H, \tag{1}$$

where $\sigma_{\xi,L}$ is the standard deviation of ξ at scale L km and H is a scale-independent parameter. Perica and Foufoula-Georgiou (1996a) found this relationship to hold within scales of 4–64 km for which observations were available. Later studies by Venugopal et al. (1999) and Harris and Foufoula-Georgiou (2001) found it to extend down to the scale of 2 km (using Next-Generation Weather Radar images) with no scaling break. Perica and Foufoula-Georgiou (1996a) also established an empirical connection between statistical and physical storm characteristics by quantifying relations between the scaling parameter H and thermodynamic or kinematic indices of the prestorm environment, such as, the convective available potential energy (CAPE), convective inhibition, bulk Richardson number, wind shear, and severe weather threat index. The best correlation was obtained with CAPE, and only a small improvement in the explained variability was achieved if other variables were included in the predictive relationship. They found that the parameter H could be predicted from CAPE ahead of the storm as

$$H = 0.052 + 0.965\ \text{CAPE} \times 10^{-4} \quad (R = 0.82), \tag{2}$$

where CAPE is in meters squared per second squared, H is dimensionless, and R is the correlation coefficient between H and CAPE. The empirical coefficients in Eq. (2) were derived from 47 selected radar scans covering mature and dissipating stages of storm development collected during the 2-month Oklahoma–Kansas Preliminary Regional Experiment for Storm-Central, field program. Thus, this relationship is considered to be applicable to midlatitude mesoscale convective systems over terrain and land use similar to the Oklahoma–Kansas region (for more details see Perica and Foufoula-Georgiou 1996a).

The relationships in Eqs. (1) and (2) allowed for the development of a new subgrid-scale rainfall disaggregation model that can statistically reproduce the rainfall variability at scales unresolved by mesoscale models while being conditioned on known large-scale rainfall averages and physical properties of the prestorm environment. In brief, a representative value of CAPE [see Zhang and Foufoula-Georgiou (1997) and section 2c of this paper] computed from the mesoscale model simulation is used to predict the value of H from Eq. (2). Then Eq. (1) is used to infer the variability of rainfall fluctuations at any scale given the variability at a reference scale (here, the grid size of the mesoscale model). Based on an inverse filtering procedure (inverse Haar wavelet transform), these fluctuations at different scales together with the initial large-scale average field can be used to reconstruct statistically the subgrid-scale rainfall variability [for details see Perica and Foufoula-Georgiou (1996b)].

It is emphasized that any rainfall downscaling scheme that can successfully reproduce the subgrid-scale rainfall variability could be used in our study in lieu of the scheme described above. However, the selected scheme offers some desirable advantages over other downscaling schemes. The most notable advantages are that the statistical characterization of downscaling [Eq. (1)] applies over a range of scales with a single parameter H (scale invariance) and that the value of H is linked to the thermodynamic properties of the prestorm environment [Eq. (2)]. The scale invariance implies a parsimonious statistical model, and the relation of the scaling

parameter H to CAPE allows its prediction from a physical variable computed in most mesoscale models. Moreover, the scaling parameter H is updated in time as the storm evolves and its CAPE changes, and this property allows the effects of subgrid-scale rainfall variability to be followed dynamically in time throughout the simulation. The selected rainfall downscaling scheme has been shown to perform well in reconstructing the percent of area covered by the storm at all subgrid scales (Perica and Foufoula-Georgiou 1996b).

Note that the grid-scale average rainfall (i.e., starting point for the downscaling scheme) and the computed values of CAPE depend on the MM5 model resolution (e.g., Zhang and Foufoula-Georgiou 1997), and thus an indirect dependence of H on the selected model resolution may result. However, Perica and Foufoula-Georgiou (1996b) have shown that the performance of the downscaling scheme in terms of reproducing the statistical structure of rainfall and its fractional coverage of rainy areas is not overly sensitive to small perturbations in CAPE; a 20% range in CAPE yielded less than 10% error in the statistical measures of the simulated (downscaled) rainfall fields. As noted in Zhang and Foufoula-Georgiou (1997), if the resolution varies within a range such that the model still adequately captures the storm dynamics, the resulting changes in the computed CAPE do not induce significant changes in the statistical structure of the downscaled fields.

c. *Coupling of the rainfall downscaling scheme to MM5–BATS*

As discussed in the previous section, CAPE is, in our downscaling scheme, the critical link between the statistical description of the subgrid-scale rainfall variability and the thermodynamic behavior of the storm environment. In a modeling system, CAPE can be computed from variables (vertical profiles of temperature, pressure, and mixing ratio of water vapor) predicted by the model at each grid point. There are several acceptable ways in which CAPE can be computed from model variables. To be consistent with the method used when the empirical relationships in Eq. (2) was derived by Perica and Foufoula-Georgiou (1996a), a surface-based CAPE was calculated at each model grid point using the formulation from the General Meteorological Package (GEMPAK; University Corporation for Atmospheric Research 1992).

The empirical relationship between the statistical characterization of multiscale rainfall variability and CAPE given by Eq. (2) is based on using a single value of CAPE describing the environment ahead of the convection. Thus, the CAPE computed within the model at each time step needs to be reduced into one storm-representative value for use in Eq. (2). Zhang and Foufoula-Georgiou (1997) introduced a representative CAPE value, denoted by $\langle \text{CAPE} \rangle$ and defined as

$$\langle \text{CAPE} \rangle = \frac{1}{N_s} \sum_{i=1}^{N} \text{CAPE}_i \times I_{K_s,i}, \tag{3}$$

where CAPE_i are the gridpoint values computed following the GEMPAK formulation, N_s is the number of grids at which CAPE_i is greater than a selected threshold value K_s, N is the total number of grid points in the model domain, and $I_{K_s,i}$ is an indicator function that is either 0 or 1 depending on whether CAPE_i is less or greater than K_s (i.e., $I_{K_s,i} = 0$ if $\text{CAPE}_i < K_s$ or $I_{K_s,i} = 1$ if $\text{CAPE}_i \geq K_s$). The value of K_s is kept fixed throughout the simulation so that changes in $\langle \text{CAPE} \rangle$ provide meaningful information on the storm evolution. The value of N_s, which depends on the preselected value of K_s, varies over time as the storm evolves.

It was observed by simulation (Zhang and Foufoula-Georgiou 1997) that the spatial distribution of CAPE tends to have higher values ahead of the convection and lower values behind it. Therefore, by selection of an appropriate threshold value K_s, the representative CAPE presented in Eq. (3) filters out lower background CAPE values and captures the CAPE ahead of the convection into a single value for use in Eq. (2). Further discussion on $\langle \text{CAPE} \rangle$ and the selection of an appropriate threshold value based on observations can be found in Zhang and Foufoula-Georgiou (1997).

The rainfall computed by MM5 at the model grid scale can now be statistically downscaled into subgrid scales as follows: (a) CAPE is computed at each of the MM5 grid points following the GEMPAK formulation, (b) $\langle \text{CAPE} \rangle$ is computed according to Eq. (3), (c) the scaling exponent H is computed from Eq. (2) using the representative value of $\langle \text{CAPE} \rangle$, (d) the standard deviation of the standardized rainfall fluctuations at the MM5 grid scale (σ_{ξ,L_1}) is computed from the MM5-predicted rainfall intensities, (e) the standard deviation of rainfall fluctuations at any scale smaller than L_1 is estimated from Eq. (1), and (f) the inverse Haar wavelet transform and Eq. (1) are used iteratively to downscale the MM5 rainfall to the desired subgrid scale. It is noted that this downscaling scheme guarantees (by its spatially localized structure) the preservation of grid-scale mean rainfall at all grids. By including some simple image-processing routines, we also ensure a realistic connectivity between wet and dry areas at the subgrid scale. That is, at each smaller scale the new subgrid values generated within each of the larger grids from the previous scale are rearranged by shifting the largest intensity to the subgrid box that is surrounded by high intensities and the smallest intensity to the subgrid box surrounded by the low intensities (Perica 1995). This rearranging improves the connectivity and spatial correlation of the subgrid-scale rainfall values to each other and to surrounding grid-scale rainfall values. The reader is referred to Perica and Foufoula-Georgiou (1996b) for more details and statistical evaluation of the downscaling scheme performance.

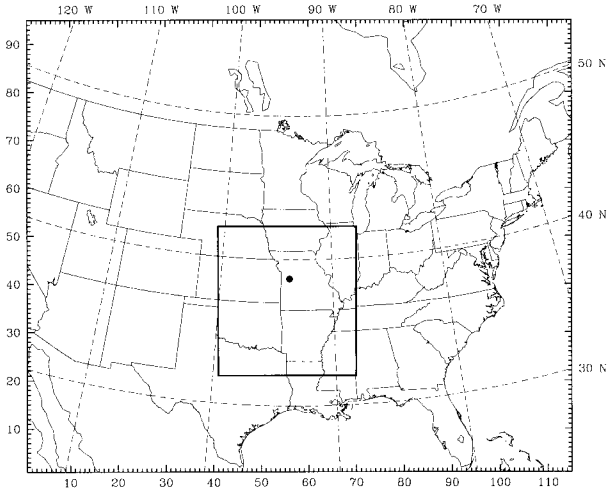

FIG. 2. Experimental setup. The MM5–BATS model was run at a grid spacing of 36 km in the outer domain (domain 1) of size 3420 km × 4140 km (94 × 114 boxes) and at a spacing of 12 km in the inner domain (domain 2, shown by the interior box) of size 1116 km × 1044 km (92 × 86 boxes). The dot inside domain 2 shows the location of the KEAX radar.

3. Numerical experiment

Assessment of the effects of subgrid-scale rainfall variability on water and energy fluxes is made in this study by comparison of a control run (called CTL) in which the MM5–BATS model does not include subgrid-scale rainfall variability with a run that includes statistically downscaled rainfall at the subgrid scale (called SRV). We emphasize that the assessment of the effect of subgrid-scale rainfall variability is done in a comparative way (i.e., with and without variability) and not by comparison with actual observations. However, instead of creating a completely hypothetical case, we have chosen to use a real storm that occurred on 4 July 1995 and is characterized as a multiple squall line event that produced severe thunderstorms and damaging winds over Kansas; a tornado in Missouri; and heavy rainfall over Oklahoma, Iowa, and northern Texas. The event lasted over 24 h, and maximum rainfall intensities were in excess of 100 mm h^{-1}. A complete description of the meteorological conditions of this 4 July 1995 event can be found in Browning et al. (1997).

The 4–5 July 1995 storm provides a good case study for investigating the effects of subgrid-scale rainfall variability and how it propagates through the coupled land–atmosphere system over time. The long duration of the storm provides a sufficient time for the subgrid-scale rainfall variability to alter the state of the land surface (e.g., soil moisture and surface temperature). The multiple-state extent of the storm provides a sufficiently large area to study the impacts on the larger-scale spatial organization of land–atmosphere fluxes. The location of the storm over the central United States corresponds to the same area for which the rainfall downscaling scheme used in this study was derived and tested in Perica and Foufoula-Georgiou (1996a). The numerical simulation of this storm was reasonable, as judged by qualitative comparison of the observed and simulated fields, although no specific attempt was made to assess quantitatively the MM5–BATS success in reproducing it. As discussed in the next section, the observed rainfall fields were only used to assess the realism of the statistical structure of the subgrid-scale rainfall variability introduced by our downscaling scheme.

TABLE 1. Model input parameters.

Initialization time	1200 UTC 4 Jul 1995
Integration time step	90 s
Simulation length	48 h
No. of vertical grid elements	32
Horizontal grid resolution	36 km, 12 km
Lateral boundary conditions	NCEP global analyses
Soil moisture initialization	Soil hydrology model (via ESSC)
Land cover, soil texture	USGS-EDC
Nesting type	Two-way interactive
Cumulus paramterization scheme	Grell

A nested grid configuration was used as shown in Fig. 2. The coarse mesh (domain 1) has a horizontal grid spacing of 36 km, and the inner nest (domain 2) has a 12-km spacing. Two-way interactive feedback was used between the domains; that is, the nest's lateral boundary conditions are provided by the coarse grid while the feedback to the coarse mesh occurs over each grid within the interior of the nest. The vertical grid consists of 32 levels, with 10 levels in the lowest 1500 m of the atmosphere. The Grell cumulus parameterization scheme, which was found by Wang and Seaman (1997) to perform well in predicting the duration and total volume of warm-season rainfall events, was used for both domains. The initial and lateral boundary conditions were generated by interpolating the National Centers for Environmental Prediction (NCEP) Early Eta Model analysis and forecast fields to the MM5 grid. Soil moisture initialization, land cover, and soil texture data files were used as input to the BATS component of the coupled MM5–BATS modeling system. For the soil moisture initialization, the three-dimensional soil water content field generated by the Soil Hydrology Model at The Pennsylvania State University Earth System Science Center (ESSC) was used. The land cover and soil texture data files were obtained from the United States Geological Survey (USGS) Earth Data Center (EDC). Topography and land surface data were provided at the 36-km resolution. A summary of the model setup and input parameters is given in Table 1. The simulation experiments of the CTL and SRV runs are described in Table 2.

4. Research methodology

a. Propagation of subgrid-scale rainfall variability through the coupled land–atmosphere system

To assess the effects of subgrid-scale rainfall variability on other variables of the water and energy cycle,

TABLE 2. Simulation experiments.

Runs	36 km	12 km	Subgrid rainfall (at 3 km)
CTL	On	On	Off
SRV	On	On	On

this variability must be allowed to propagate through the coupled land–atmosphere system at the scale at which it was imposed. In this study, the statistically downscaled rainfall is used as input into the BATS component of the coupled model, which is run at a resolution equal to the resolution of the downscaled rainfall. The prescribed subgrid-scale variability of rainfall propagates through the linear and nonlinear equations of BATS [e.g., see Dickinson et al. (1993) and Yang and Dickinson (1996) for these equations] to produce subgrid-scale variability in other land surface variables. Through the two-way interactive coupling of MM5 and BATS, the resulting variability in the land surface variables feeds back to the atmosphere.

Figure 3 shows a schematic of the subgrid-scale implementation used in the SRV run along with the original MM5–BATS coupling used in the CTL run. Within domain 2, MM5 is run at the grid scale of 12 km, and the rainfall downscaling and BATS are run at a finer 3-km subgrid scale. This was done by redistributing the BATS input variables to the 3-km subgrids within each of the 12-km grid boxes. To isolate the effects of the subgrid-scale rainfall variability, the other BATS input variables (e.g., soil properties, initial soil moisture, temperature, pressure) were homogeneously distributed within the 12-km boxes at the beginning of the simulation; that is, the resolvable grid-scale value of these variables was used for each subgrid box contained within the MM5 grid box. At later time steps, the subgrid-scale variables simulated by BATS (e.g., soil moisture, surface temperature, surface fluxes) were allowed to evolve in response to the imposed subgrid-scale rainfall variability.

To be used by MM5 at the next time step, the BATS variables were returned to MM5 by averaging over the subgrid back to the resolvable MM5 grid scale. The subgrid-scale values of the BATS variables that were not altered by MM5 were kept for input at the next time step. The BATS subgrid-scale variables that were altered by MM5 were linearly adjusted at the next time step to preserve the new MM5 grid-scale average. This was done to preserve the grid-scale water and energy budgets produced by MM5 while maintaining the subgrid-scale variability and spatial distribution of these variables.

Implementing BATS on the subgrid scale and then areally averaging its output variables back to the 12-km grid to be used by MM5 for the next time step allows for the temporal propagation of the subgrid-scale rainfall variability through the nonlinear land–atmosphere system to be followed in a dynamical way. That is, explicitly incorporating this subgrid-scale variability within BATS and its nonlinear feedback to MM5 at the grid scale affect how the coupled land–atmosphere system evolves over time. Although the variability is applied at the subgrid scale, the effects are viewed back at the larger MM5 grid scale such that comparisons can be made with the MM5 control run that did not include subgrid-scale rainfall variability.

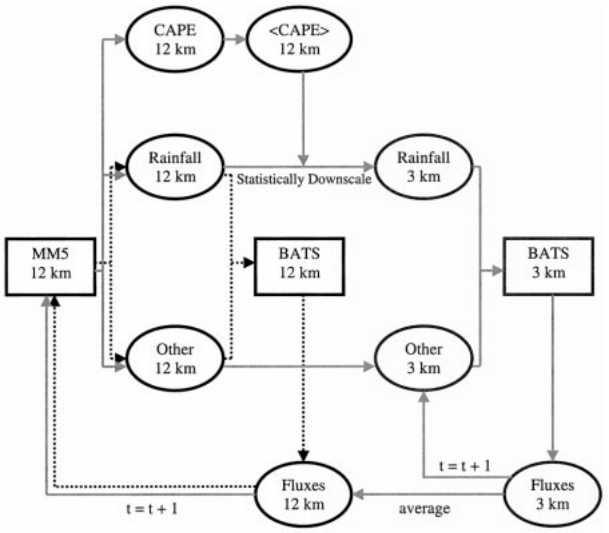

FIG. 3. Schematic of the subgrid-scale implementation of MM5–BATS. The dashed arrows show the flow of the original MM5–BATS coupled model. The solid arrows show the flow of the subgrid implementation of the MM5–BATS coupled model.

b. Ensemble simulations

Because the scheme used for downscaling rainfall is statistically driven, each subgrid-scale rainfall field is one realization of a realm of possible fields that can be generated from the same large-scale average values and the storm environmental parameters such as CAPE. To assure that the effects we see are not artifacts of one particular realization but are truly coming from the interaction of the subgrid-scale rainfall heterogeneities and the dynamics of the land–atmosphere system, a 15-member ensemble of SRV runs was created by generating different realizations of standardized rainfall fluctuations [from normal distributions of zero mean and standard deviations specified by Eq. (1)] for use in the downscaling scheme. If everything else is kept the same, each realization of subgrid-scale rainfall will propagate through the nonlinear system of equations in a different way and will result, at a later time and at the same grid box, in different values of the land–atmosphere variables, for example, latent and sensible heat fluxes.

For the effects of subgrid-scale rainfall variability to be judged, as statistically significant, the difference between the CTL run and the average of the ensemble of SRV runs must be outside the statistical variability of the ensemble. Here, statistically significant differences

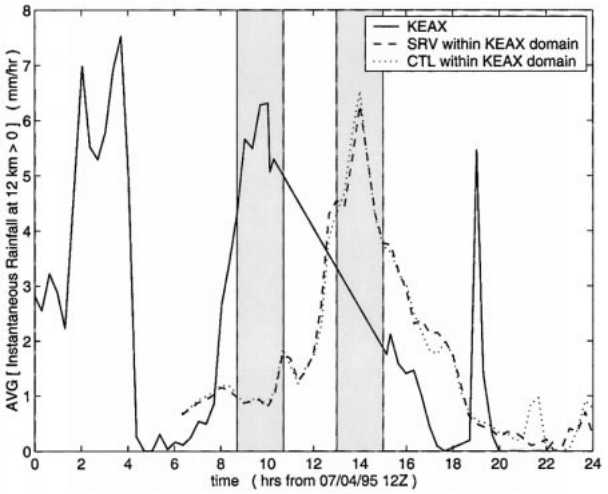

FIG. 4. Nonzero instantaneous rainfall observed within the KEAX radar domain (solid line) and the same for the MM5-simulated rainfall without downscaling (dotted line) and with downscaling (dashed line). Notice that the model offsets the simulated peak by approximately 4 h. Comparison of the multiscale variability of the observed and downscaled rainfall was performed within the shaded 2-h periods centered around the peaks.

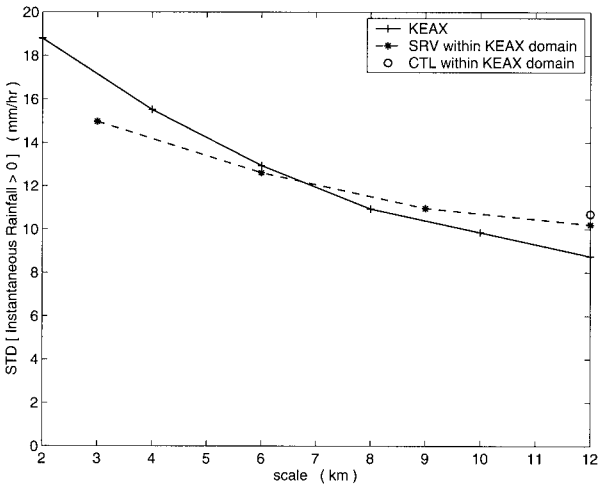

FIG. 5. Comparison of multiscale variability of observed and MM5-modeled and -downscaled instantaneous rainfall. The values shown are averages over a 2-h period around the peak rainfall rate (see Fig. 7). The solid line corresponds to the rainfall observed within the KEAX radar domain and the dashed line to the MM5-simulated rainfall with downscaling (SRV run). At the model grid scale of 12 km, the standard deviation of the MM5-simulated rainfall without downscaling (CTL run) is also shown in the figure (circle).

were denoted as any differences that are outside the range of the mean plus/minus one standard deviation of the ensemble, that is, differences for which

$$|\overline{\text{SRV}} - \text{CTL}| > \sigma_{\text{SRV}}. \quad (4)$$

The results from the SRV ensemble runs were found to be statistically and physically similar, with spread among them much smaller than the spread between any member of the ensemble and the control run. This result provided reassurance that the effects of including subgrid-scale rainfall variability and accounting for its nonlinear propagation through the land–atmosphere system were not merely artifacts of one particular realization of downscaled rainfall. The accumulated rainfall and upper-layer relative soil moisture SRV ensemble results are discussed later, in section 5a (Figs. 7e,f). More results from the ensemble simulations can be found in Nykanen (2000).

c. Subgrid-scale rainfall verification

Because conclusions related to the effects of subgrid-scale rainfall on other variables in a coupled land–atmosphere scheme hinge on how realistic the introduced subgrid-scale rainfall variability is, here an attempt is made to verify that the subgrid-scale rainfall variability added in the SRV run is reasonable when compared with the observed subgrid-scale variability. For that purpose, 2-km-resolution observed rainfall from the KEAX radar located at Pleasant Hill, Missouri, was compared with the subgrid-scale rainfall added via downscaling in the SRV run within the 256 km by 256 km KEAX coverage area.

Comparisons of rainfall intensities between the model and observations showed that MM5 was able to capture reasonably the spatially averaged peak rainfall intensity but with an offset of almost 4 h (see Fig. 4). No attempt was made in our study to synchronize the peaks and optimize the performance of MM5, because this offset is of no consequence when the fluxes simulated by the CTL and SRV runs are compared with each other but not with the actual observed fluxes. However, to compare the subgrid-scale variability of downscaled and observed rainfall, the large-scale averages have to be of comparable magnitude. For this reason, we concentrated on a 2-h period centered around the observed and simulated peak rainfall (see Fig. 4) and compared the multiscale variability (2–12 km for radar and 3–12 km for model-predicted rainfall). Figure 5 demonstrates that the subgrid-scale variability introduced is realistic and is similar to that of the actual rainfall fields. If anything, the introduced variability is seen to be less than that observed and therefore the impacts of accounting for small-scale rainfall variability might be even larger than the ones reported in this study.

Figure 6 shows the temporal evolution of the representative CAPE ($\langle$CAPE$\rangle$) and the scaling parameter H for the 4–5 July 1995 storm as simulated by the SRV run. The $\langle$CAPE$\rangle$ and consequently H [as computed by Eq. (2)], followed well the dynamical evolution of the storm as it passed through domain 2. The first peak at $t = 11$ h captures the storm that moved through the northern half of the domain, and the second peak at $t = 17$ h captures the storm that moved through the southern half of the domain. When the rainfall moves out of

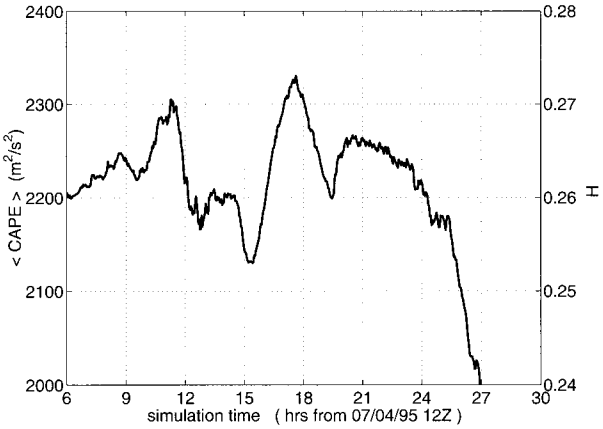

FIG. 6. Time evolution of ⟨CAPE⟩ and H for the 4–5 Jul 1995 storm as simulated by the SRV run.

domain 2 at approximately $t = 27$ h, the ⟨CAPE⟩ and H parameters rapidly decrease.

5. Results

a. Anomalies in model-predicted variables

The effects of including or omitting the subgrid-scale variability of rainfall on other variables of the water and energy cycle simulated through the coupled land–atmosphere system were quantified by comparing the CTL and SRV model simulations. Differences between the CTL and SRV runs are referred to as ''anomalies'' and are expressed as SRV minus CTL. It is emphasized that, although the rainfall variability was applied at the 3-km subgrid scale, the results or effects of including this variability were assessed back at the 12-km model grid scale.

Rainfall occurred during the simulation from approximately $t = 9$ until $t = 27$ h producing peak accumulations that exceed 100 mm. Peak hourly rainfall rates exceeded 40 mm h^{-1} as the storm passed over Missouri, Arkansas, and southeastern Oklahoma. The total rainfall accumulated at 27 h into the simulation is shown for the CTL run in Fig. 7a. The relative soil moisture in the upper soil layer (top 10 cm) is shown in Fig. 7b for the CTL run at $t = 27$ h. Anomalies, or differences, between the CTL and SRV accumulated rainfall and soil moisture are shown in Figs. 7c–f. The results for one member of the ensemble are shown in Figs. 7c and 7d, where the anomalies were computed as $SRV_1 -$ CTL. Figures 7e,f show the results for the ensemble average and are masked to display only the anomalies outside plus/minus one standard deviation of the SRV ensemble according to Eq. (4).

The anomalies in total accumulated rainfall grew and organized as the storm progressed. The red shaded areas indicate where the SRV run produced more rainfall than the CTL run (SRV $>$ CTL: positive anomalies) and the blue shaded areas indicate where the SRV run produced less rainfall than the CTL run (SRV $<$ CTL: negative anomalies). The adjacent patches of positive and negative anomalies of approximately the same magnitude are evidence of a shifting in the location of rainfall between the SRV and CTL runs. Patches of more intense increase or decrease in comparison with surrounding patches reveal changes in magnitude of rainfall accumulation between the SRV and CTL runs.

It can been seen from Figs. 7c–f that any one member of the ensemble produces very similar anomalies as compared with the ensemble average. There are some minor differences, but the overall trends in size, shape, and magnitude of the larger-scale spatial organization of the anomalies is similar. With this verification, further discussion of the results will focus on one member of the SRV ensemble rather than carrying all the ensemble members throughout the analysis. Figure 7 provides evidence that including subgrid-scale rainfall variability and its nonlinear propagation through the land–atmosphere system had a statistically significant effect on the spatial organization of accumulated rainfall and upper-layer relative soil moisture.

The sign of the large-scale anomalies produced in the soil moisture by accounting for the subgrid-scale variability of rainfall can be related to the anomalies in the accumulated rainfall and the process dominating the soil water balance and the nonlinear shape of its parameterization (i.e., concave or convex). By comparing the sign of the anomalies with the magnitude of the soil moisture field, it was found that negative anomalies tend to occur where the soil is wet and positive anomalies occur where the soil is dry. Figure 8 shows in a schematic the shapes of the surface runoff and maximum sustainable transpiration rates as a function of relative soil moisture as parameterized in BATS [$R_s \propto s^4$ and $\max E_{tr} \propto 1 - (s^{-B} - 1)/(s_{wilt}^{-B} - 1)$, where R_s is surface runoff, s is the relative soil moisture, s_{wilt} is the relative soil moisture at which permanent wilting occurs and transpiration ceases, and B is the Clapp–Hornberger soil parameter]. From this figure it is evident that including subgrid-scale rainfall variability, which produces subgrid-scale soil moisture variability, will result in different signs of the anomalies at the grid scale depending on the dominant process. When the soil is wet ($s \geq 0.6$) and surface runoff is the dominant process, Fig. 8a shows that more water is removed by including subgrid-scale variability, which means that less water will remain in the soil (i.e., negative soil moisture anomaly). Figure 8b shows that, when the soil is dry ($s \leq 0.6$) and transpiration is the dominant process, less water is removed from the soil by including subgrid-scale variability, which means that more water will remain in the soil (i.e., positive soil moisture anomaly). This conclusion is supported by Fig. 9, which shows the average upper-layer relative soil moisture in the CTL run for areas where positive and negative anomalies greater than a specified threshold are located. This figure demonstrates that the average soil moisture under positive

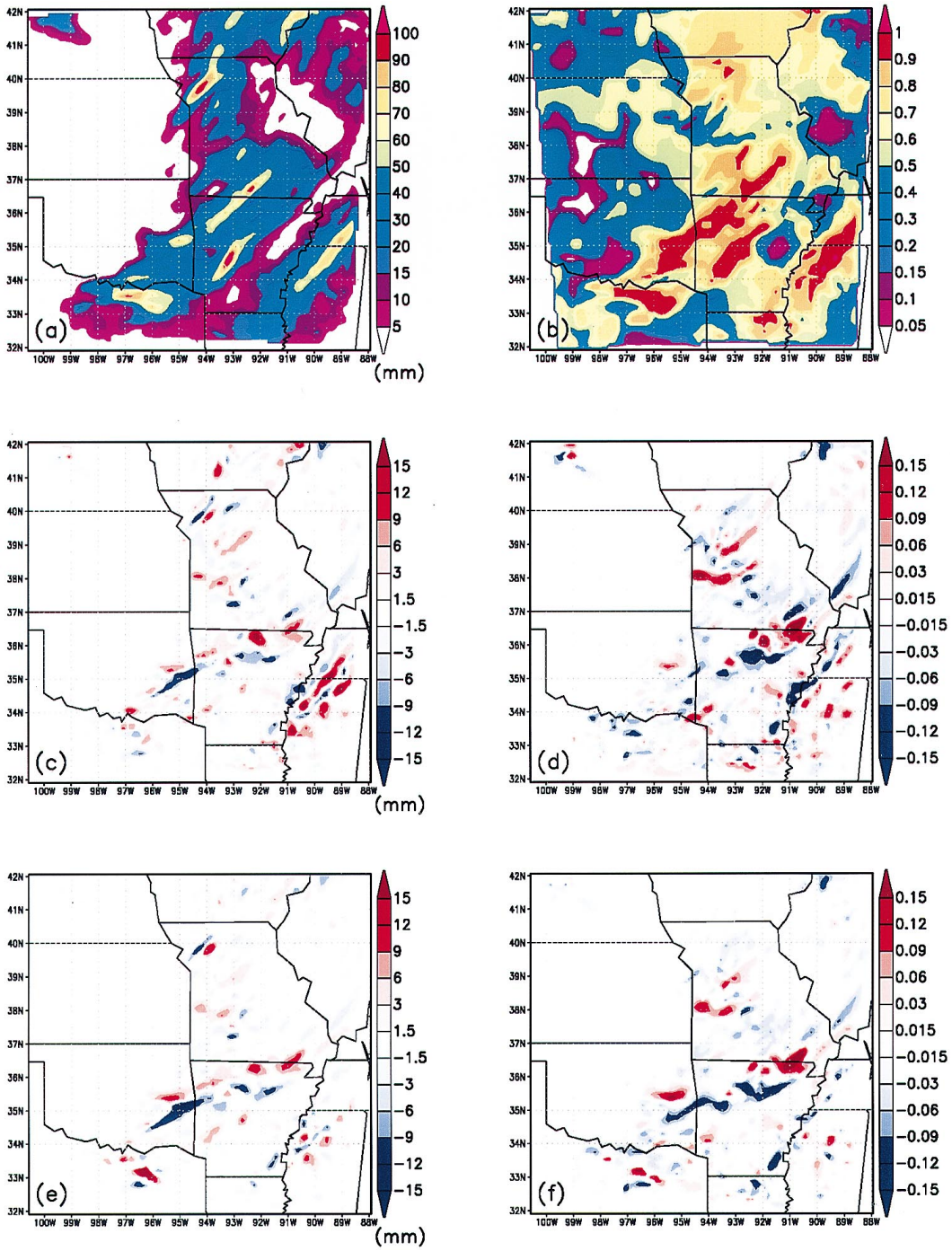

FIG. 7. (a) Accumulated rainfall and (b) relative soil moisture in the upper soil layer for the CTL run at $t = 27$ h into the simulation. (c) Accumulated rainfall and (d) relative soil moisture in the upper soil layer at $t = 27$ h with anomalies computed as SRV1 − CTL, where SRV1 is one member of the SRV ensemble. (e) Accumulated rainfall and (f) relative soil moisture in the upper soil layer at $t = 27$ h with anomalies computed at $\overline{\text{SRV}}$ − CTL and masked to show only those for which $|\overline{\text{SRV}} - \text{CTL}| > \sigma_{\text{SRV}}$, where $\overline{\text{SRV}}$ and σ_{SRV} are the average and standard deviation of the ensemble members, respectively.

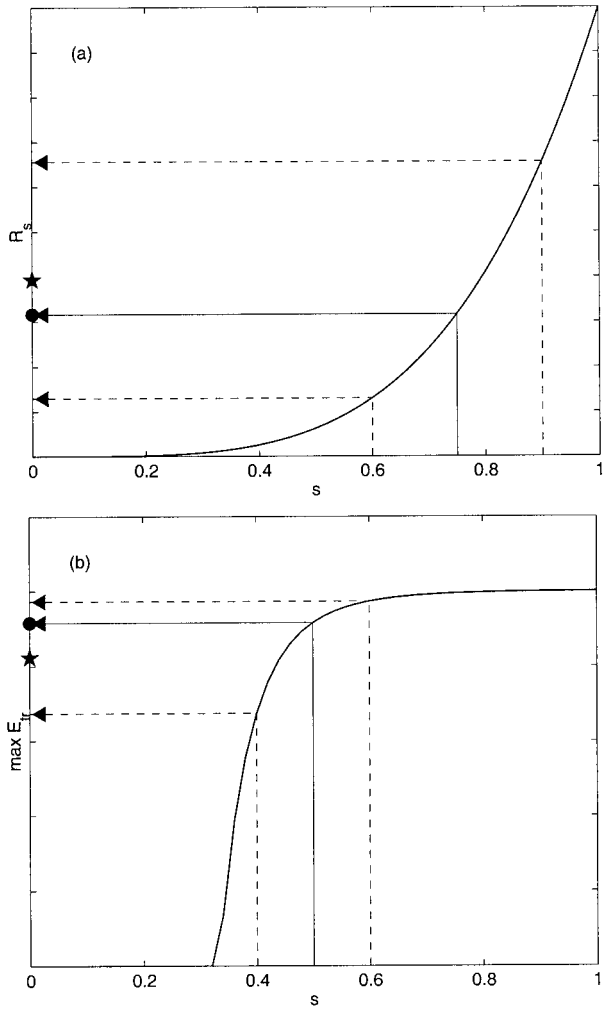

FIG. 8. Schematic illustrating the nonlinear shape of the surface runoff R_s and maximum sustainable transpiration rate maxE_{tr} parameterizations used in BATS as a function of relative soil moisture s. The filled circle corresponds to $F(\bar{s})$ and the star corresponds to $\overline{F(s)}$. (a) The concave, nonlinear shape of the surface runoff parameterization gives $\overline{F(s)} > F(\bar{s})$. (b) The convex, nonlinear shape of the maximum sustainable transpiration rate gives $\overline{F(s)} < F(\bar{s})$.

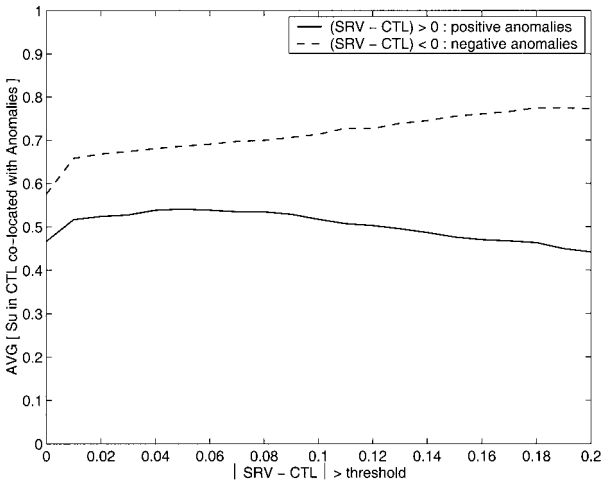

FIG. 9. Average of the upper-layer (top 10 cm) relative soil moisture S_u in the CTL run for areas where positive and negative anomalies (i.e., SRV − CTL) greater than a specified threshold are located. The average is computed in space (over domain 2 where anomalies occur) and in time (from t = 20 to 36 h). The solid line corresponds to positive anomalies, and the dashed line corresponds to negative anomalies. This figure supports the conclusion that negative anomalies tend to occur where the soil is wet and positive anomalies occur where the soil is dry.

anomalies was consistently drier than that under negative anomalies. Figure 10 illustrates that including subgrid-scale rainfall variability has decreased the area of near-saturated soil. This figure further supports the conclusion that, in wet soil where surface runoff is the dominant process, the nonlinear propagation of subgrid-scale rainfall variability through the surface runoff parameterization results in increased surface runoff and, consequently, a negative soil moisture anomaly.

To assess the effects of including subgrid-scale rainfall variability on other variables of the water and energy cycles, several surface variables modeled by the coupled land–atmosphere system were compared between the CTL and SRV runs. It was found that accounting for the subgrid-scale rainfall variability and the small-scale nonlinear feedbacks produced anomalies in the upper-layer soil moisture, surface temperature, and sensible and latent heat fluxes from the surface as shown in Fig. 11. By following the anomalies over time, it was found that they grew and spatially organized into patches of size much larger than the 3-km scale at which the rainfall variability was prescribed. Anomalies in the temperature, sensible heat flux, and latent heat flux of the surface were found to grow and to dissipate with the diurnal cycle. Anomalies in the surface soil moisture grew during the rainfall period and then persisted throughout the rest of the simulation, illustrating the long memory of soil moisture anomalies. For brevity, the surface variable anomalies are only shown at t = 32 h into the simulation in Fig. 11.

b. Spatial and temporal organization of anomalies

The spatiotemporal organization of the anomalies was quantitatively characterized by computing their spatial and temporal correlations and average size of anomaly patches above a threshold. It is emphasized that the following observations and discussion refer to anomalies that resulted from including or omitting subgrid-scale rainfall variability.

Figure 12 shows the cross-correlation coefficient computed from synchronized anomaly fields (time lag 0 h) of several model-predicted surface variables throughout the simulation. The effects of the diurnal cycle on the anomalies is evident in Fig. 12a, with the cross correlation between the surface temperature anomalies and surface heat fluxes anomalies being negative during the nighttime hours and positive during the day-

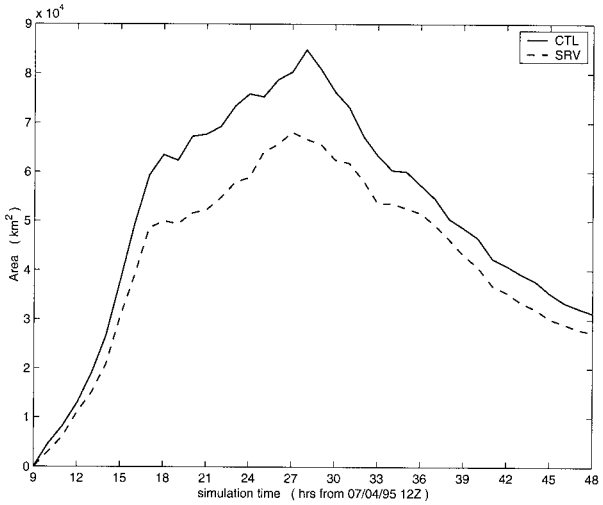

FIG. 10. Area with upper-layer (top 10 cm) relative soil moisture greater than or equal to 0.9 (i.e., 90% saturated). The CTL (solid line) run produced significantly more area of near-saturated soil than did the SRV (dashed line) run, illustrating that accounting for the nonlinear propagation of subgrid-scale rainfall variability through the surface runoff parameterization results in more surface runoff in wet soils and, consequently, negative soil moisture anomalies.

time. The cross-correlation coefficient between the sensible and latent heat flux anomalies also followed the diurnal cycle. Figure 12b shows the strong, positive correlation between the anomalies in the soil moisture and accumulated rainfall. As expected, the correlation between the anomalies in antecedent rainfall (past 3 h) and the soil moisture dies off as the rainfall ceases, and the correlation between the anomalies in the soil moisture and latent heat flux from the surface grows throughout the simulation as the soil becomes more saturated.

To follow how the anomaly fields of each variable change over time, the cross-correlation coefficients were computed for each anomaly field with the same variable anomaly field at a previous time. Starting at $t = 20$ h, for example, the cross correlation was computed between the anomaly field at $t = 20$ h and the anomaly fields of the same variable at $t = 19$ h, $t = 18$ h, and $t = 17$ h. This computation resulted in a temporal autocorrelation function of each field that depicted the temporal persistence of the anomalies. The temporal autocorrelation length is defined here as the time lag in hours at which the correlation coefficient dropped below 0.3. The autocorrelation length for three different starting times selected to depict the ''during'' and ''after'' rainfall and ''day'' and ''night'' conditions are shown in Fig. 13. The accumulated rainfall and upper-layer soil moisture anomalies grew throughout the simulation as the storm evolved, and, as shown by Fig. 13, they exhibited the longest temporal autocorrelation length (i.e., longest memory) among the various surface variables. It can also be seen from Fig. 13 that the temporal autocorrelation length for the surface temperature and sensible and latent heat fluxes depended both on the diurnal cycle and on the storm evolution, with the correlation length being the longest during the night and after the storm ended.

The anisotropy of the spatial correlation of the anomalies in the model-predicted surface variables was also computed throughout the simulation. The spatial correlation length, defined as the lag at which the spatial correlation coefficient drops below 0.3, was found to be approximately 40 km for anomalies in the upper-layer soil moisture, surface temperature, sensible and latent heat fluxes, and accumulated rainfall. The orientation of maximum spatial correlation length was found to be southwest–northeast (i.e., 45°) for the soil moisture and accumulated rainfall anomalies, which is perpendicular to the overall direction in which the rainfall-producing storm cells were moving. The spatial correlation of anomalies in the surface temperature and surface heat fluxes were found to be almost isotropic, with a maximum in the south–north (i.e., 90°) orientation.

Histograms of the patch sizes in the anomalies were computed for various thresholds on the magnitude of the anomalies to determine the spatial organization and size distribution of the patches. Figure 14 shows the histogram of patch sizes above a specified threshold for anomalies in upper-layer relative soil moisture, surface temperature, and sensible and latent heat fluxes from the surface. The average and maximum sizes of the spatially organized anomaly patches versus threshold are given in Figs. 15 and 16, respectively. The solid line corresponds to positive anomalies (SRV $>$ CTL) and the dashed line to negative anomalies (SRV $<$ CTL). Figures 15a–d quantify that the average sizes of positive anomalies are comparable to those of negative anomalies in each of the variables except in upper-layer relative soil moisture, which tends to have much larger negative anomalies for small thresholds on soil moisture. However, the maximum size of anomaly patches seems to be overwhelmingly coming from positive anomalies in surface temperature and sensible and latent heat fluxes during the day (see Figs. 16b–d). This result indicates that omitting small-scale rainfall variability can result in this situation in incorrect simulation of persistent large regions of colder surface temperatures and lower sensible and latent heat fluxes. Figures 16b–d illustrate that during the day the anomalies in surface temperature and sensible and latent heat fluxes from the surface are positive and are strongly spatially organized. Figures 14–16 provide evidence that the anomalies produced in the surface variables by including or omitting subgrid-scale variability in rainfall are spatially organized and are grouped in patches of size much larger than the model grid resolution. It is noted that [even if the average sizes and magnitudes of positive and negative anomalies are comparable (see also visually from Fig. 11) and therefore over the whole domain their effect can be seen as canceling] for a particular watershed of size as small as 1000 km^2 the location of these anomalies

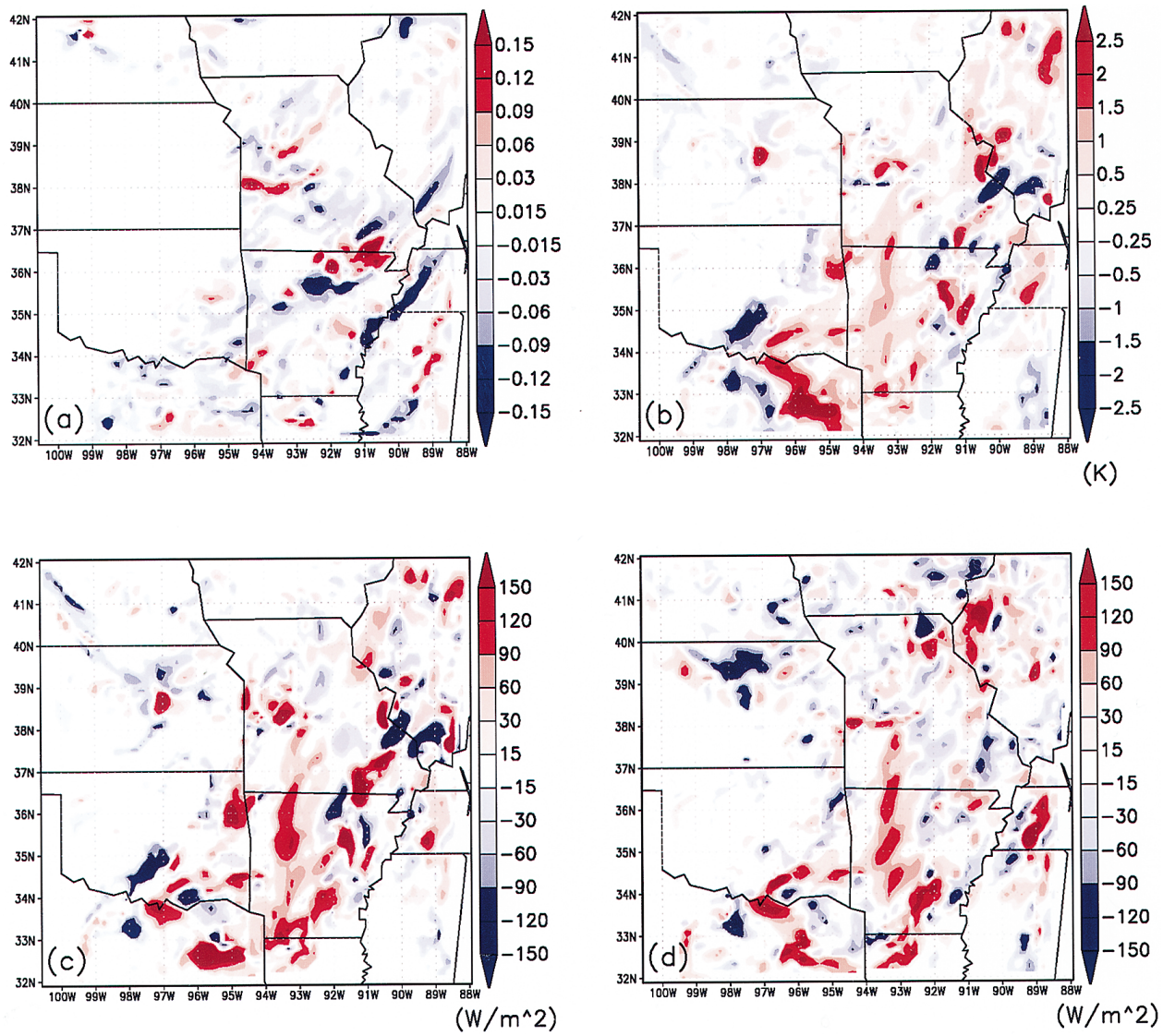

FIG. 11. Anomalies (SRV − CTL) at $t = 32$ h into the simulation (1500 local time) for (a) relative soil moisture in the upper soil layer (S_u), (b) surface temperature (TG), (c) sensible heat flux from the surface (HFX), and (d) latent heat flux from the surface (QFX).

can result in large differences on predicted runoff from the watershed.

c. Discussion

Recent research on land–atmosphere feedback mechanisms (Brubaker and Entekhabi 1996 and Bonan and Stillwell-Soller 1998) has demonstrated that there exists a strong negative correlation between soil moisture and temperature anomalies. Figure 12a shows the presence of this negative correlation between anomalies in surface soil water content and surface temperature produced by including or omitting subgrid-scale rainfall variability. Figure 12a also shows a positive correlation between anomalies in the sensible and latent heat flux with the surface temperature during the day. As shown in Fig. 11, the anomalies are spatially organized and grouped in patches of size much larger than the scale at which the rainfall variability was prescribed, and they behave according to the physical relationships between the various surface variables. This result gives confidence that the effects are due to the land–atmosphere feedbacks and that the subgrid-scale rainfall variability invokes systematic changes in other surface variables through the nonlinear relationships of the land–atmosphere system.

The soil moisture state plays a critical role in many land–atmosphere feedback mechanisms. For example, the percent of saturation condition of the soil alters the partitioning of rainfall into infiltration and runoff. Although not specifically modeled and quantified in this study, it can be seen from Fig. 11a that the anomalies

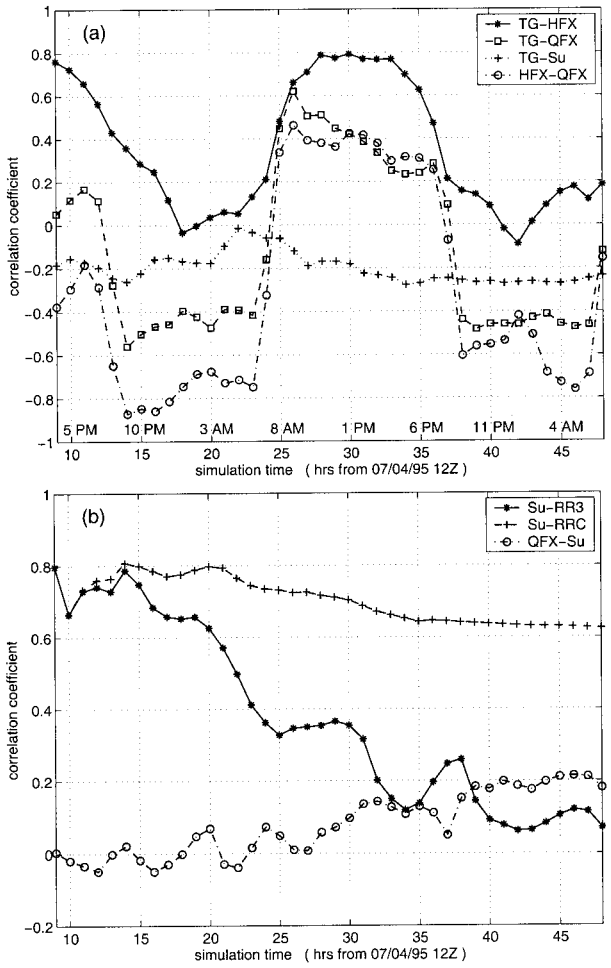

FIG. 12. Cross-correlation coefficient of synchronized anomaly fields (time lag 0 h) throughout the simulation. The surface variables shown are defined in Table 3.

TABLE 3. Surface variables.

S_u	Upper-layer (top 10 cm) relative soil moisture
TG	Surface temperature
HFX	Sensible heat flux from the surface
QFX	Latent heat flux from the surface
RR1	1-h accumulated rainfall
RR3	3-h accumulated rainfall
RRC	Total accumulated rainfall

produced in the surface soil water content by including subgrid-scale rainfall variability will affect the runoff generated in these regions. Numerous studies have shown that the soil moisture state also influences the energy budget through the interactions between the land and the atmosphere (see Camillo et al. 1983; Siebert et al. 1992; Brubaker and Entekhabi 1996; Porporato et al. 2000; among others). The availability of excess surface soil water content increases evaporation and the latent heat flux and cools the surface, whereas dry soil results in warmer temperatures and increased sensible heat flux so as to maintain a balance in the energy budget. The state of the soil moisture thus strongly influences the partitioning of incoming solar energy between sensible and latent heat.

Brubaker and Entekhabi (1996) compared the coupled land–atmosphere response to cool/moist and warm/dry anomalous initial states of the soil moisture and temperature. They found that the surface water and energy balances are in direct competition for restoring soil moisture and temperature anomalies. When considered separately, the soil water and soil energy balances each have strong self-restoring forces. However, when considered simultaneously in a coupled land–atmosphere system, they act against each other's self-restoring forces and instead further enhance the cool/moist or warm/dry condition (Brubaker and Entekhabi 1996). Although the anomalies found in our study are produced in a completely different way (i.e., by including or omitting subgrid-scale variability in the rainfall), Fig. 12a shows a similar competition between the soil water and energy balances' self-restoring forces. During the day, the energy budget controls the partitioning between latent and sensible heat fluxes, and the energy budget's demand to cool the warm (positive) anomalies is stronger than the soil water budget's demand to retain the current moisture in the dry (negative) anomalies. At night, the sensible heat flux anomalies shut down, because there is no solar radiation to drive the heat flux and the water budget's demand to retain moisture in the dry (negative) anomalies and remove excess moisture in the wet (positive) anomalies is stronger than the energy budget's demand for cooling in warm/dry soil and warming in cool/wet soil. Figure 12a shows that the correlation between anomalies in surface temperature and sensible heat flux-

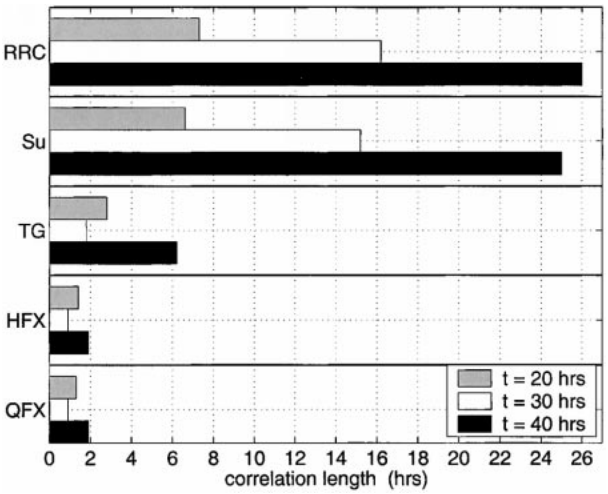

FIG. 13. Temporal autocorrelation length (in hours) of anomalies depicting the temporal persistence (i.e., memory) of anomalies (see text for details of computation). The selected starting times correspond to: $t = 20$ h (during rain, night conditions), $t = 30$ h (during rain, day conditions), and $t = 40$ h (after rain, night conditions). The surface variables shown are defined in Table 3.

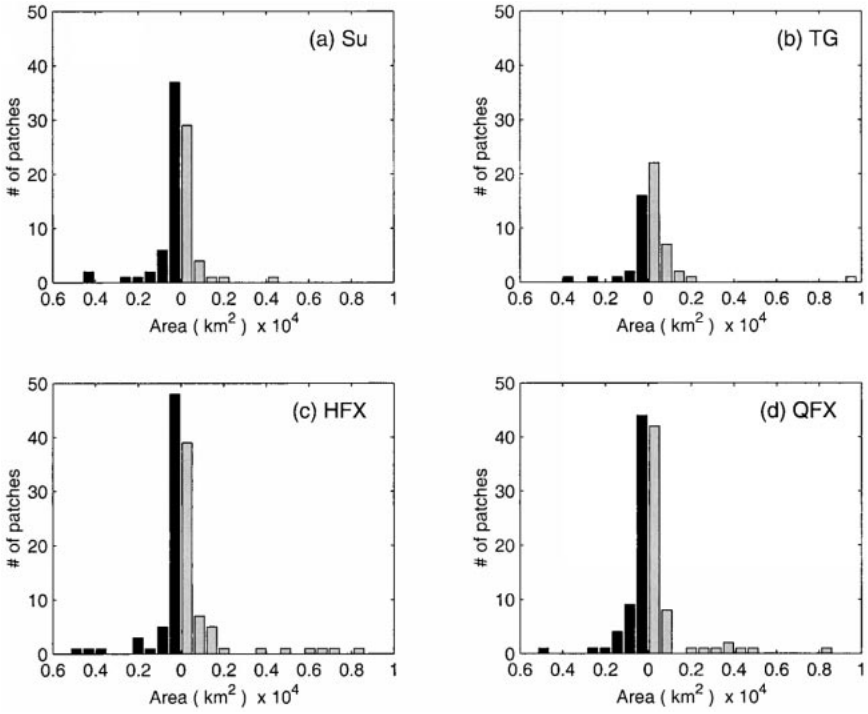

FIG. 14. Histogram of the patch sizes in anomalies at $t = 32$ h into the simulation for anomaly magnitudes of (a) relative soil moisture in the upper soil layer (S_u) > 0.10, (b) surface temperature (TG) > 2.0 K, (c) sensible heat flux from the surface (HFX) > 100 W m^{-2}, and (d) latent heat flux from the surface (QFX) > 100 W m^{-2}. The gray bars correspond to positive anomalies (SRV $>$ CTL) and the black bars correspond to negative anomalies (SRV $<$ CTL).

es from the surface is stronger during the day than at night. This result is due to solar radiation being needed to drive the heat fluxes and also reflects the strong self-restoring forces of the energy budget during the day.

6. Concluding remarks

Our study suggests that small-scale (less than 10–15 km) heterogeneities in rainfall tend to create, through the feedbacks of the land–atmosphere system, larger-scale (greater than 15 km) heterogeneities in soil moisture that further amplify the effects of the land surface on energy redistribution and rainfall production at the mesoscale. It was found that the 3-km rainfall heterogeneities propagate to larger-scale heterogeneities in total accumulated rainfall, soil moisture, surface temperature, and sensible and latent heat fluxes from the surface. The anomalies were found to be spatially organized and grouped in patches of size much larger (length scale of approximately 40 km) than the subgrid scale of 3 km at which the rainfall variability was prescribed. This result suggests that the anomalies are due to the land–atmosphere feedbacks and that the subgrid-scale rainfall variability invokes systematic changes in other surface variables through the nonlinear relationships of the land–atmosphere system.

One should remember that the rainfall variability was applied at the 3-km subgrid scale but that the results were viewed back at the 12-km model grid. The differences found here imply that, even if the scale of interest is resolvable by the model physics (here the 12-km scale of the MM5 model), the effects of subgrid-scale rainfall variability and its interactions with other variables at the subgrid scale are still important and should be considered further. These results emphasize the potential importance of accounting for subgrid-scale rainfall variability even if the interest is in larger-scale predictions. The anomalies in model-predicted soil moisture, surface temperature, and surface heat fluxes produced by including subgrid-scale rainfall variability and its propagation through the land–atmosphere relationships and through time were found to be statistically significant and to have a physically explainable spatial and temporal organization. The anomalies (between including and omitting subgrid-scale rainfall variability) were judged to be statistically significant in the sense that they were outside the range of statistical variability of an ensemble of runs, all of which included subgrid-scale rainfall variability.

It is noted that two other model configurations were analyzed to assess whether the results were dependent on the subgrid scale at which the rainfall variability was prescribed and on the model grid resolution. These configurations were (a) 36-km outer domain with 9-km sub-

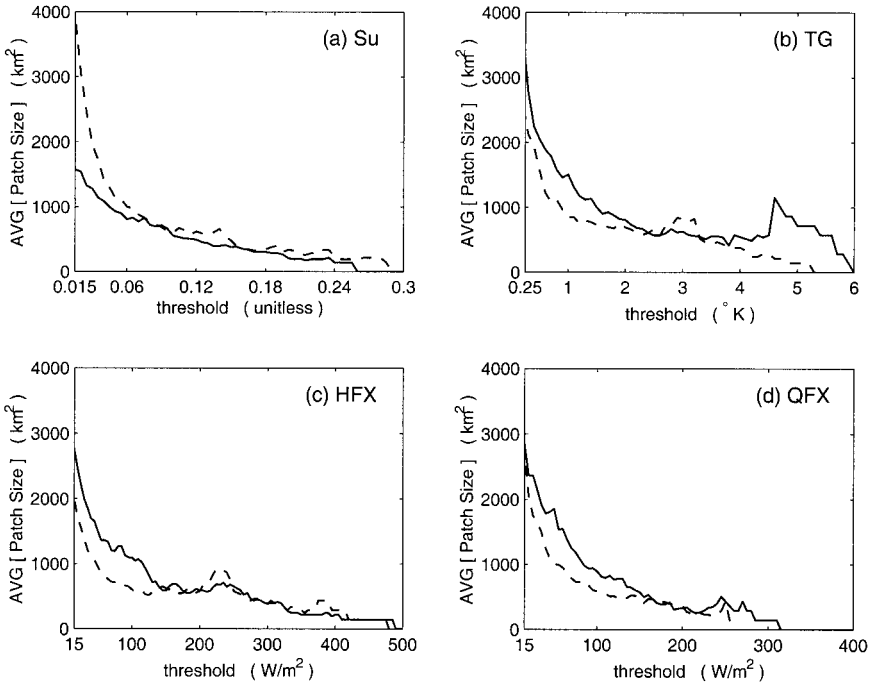

FIG. 15. Average size of spatially organized patches above a given threshold for anomalies in (a) relative soil moisture in the upper soil layer (S_u), (b) surface temperature (TG), (c) sensible heat flux from the surface (HFX), and (d) latent heat flux from the surface (QFX) at $t = 32$ h into the simulation. The solid line corresponds to positive anomalies (SRV > CTL) and the dashed line corresponds to negative anomalies (SRV < CTL).

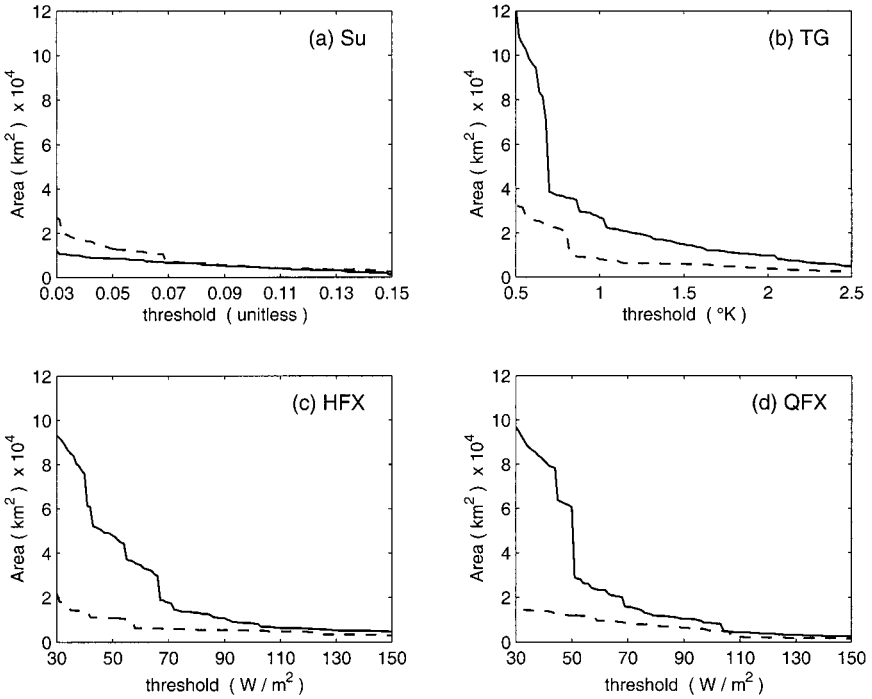

FIG. 16. Area of the largest spatially organized patch above a given threshold for anomalies in (a) relative soil moisture in the upper soil layer (S_u), (b) surface temperature (TG), (c) sensible heat flux from the surface (HFX), and (d) latent heat flux from the surface (QFX) at $t = 32$ h into the simulation. The solid line corresponds to positive anomalies (SRV > CTL) and the dashed line corresponds to negative anomalies (SRV < CTL).

grid-scale rainfall variability over the whole domain and (b) 36-km outer domain with 12-km inner nested domain and 6-km subgrid-scale rainfall variability over the inner domain. The results of these simulations exhibited similar trends in the spatial and temporal organization in the anomalies and had similar physical explanations as the results presented herein.

Our study quantified only the effects of subgrid-scale variability of rainfall by keeping the vegetation type, soil texture, and topography constant over the grid. Future research should explore resolving these land surface variables at a finer spatial resolution in addition to including the subgrid-scale rainfall variability. The combined effects of subgrid-scale spatial variability of more than one interacting variable could amplify or dampen the effects found in this study. This issue needs to be investigated. Future research should also include investigation of the relative importance of the effects of subgrid-scale rainfall variability as compared with the effects produced by uncertainties in the initial conditions, boundary conditions, or other stochastic forcings of the atmosphere and land surface state (e.g., Warner et al. 1997; Li et al. 1995; Chu 1999; Stensrud et al. 2000). If the anomalies found here by including subgrid-scale rainfall variability are comparable in magnitude and size to anomalies produced by perturbations in the model physics and initial and lateral boundary conditions, it could have potential implications in how ensembles can be generated and in quantifying uncertainty of predictions.

Acknowledgments. This research has been funded by the GEWEX/GCIP program and the NASA Land Surface Hydrology program under NASA Grant NAG8-1519. The first author gratefully acknowledges the support of a USDA National Needs Fellowship in Water Science. Computer resources were kindly provided to us by the Minnesota Supercomputing Institute. We thank two anonymous reviewers for their useful comments.

REFERENCES

Bonan, G. B., and L. M. Stillwell-Soller, 1998: Soil water and the persistence of floods and droughts in the Mississippi River Basin. *Water Resour. Res.,* **34,** 2693–2701.

Browning, P., J. F. Weaver, and B. Connell, 1997: The Moberly, Missouri, tornado of 4 July 1995. *Wea. Forecasting,* **12,** 915–927.

Brubaker, K. L., and D. Entekhabi, 1996: Analysis of feedback mechanisms in land–atmosphere interaction. *Water Resour. Res.,* **32,** 1343–1357.

Camillo, P., R. Gurney, and T. Schmugge, 1983: A soil and atmospheric boundary layer model for evapotranspiration and soil moisture studies. *Water Resour. Res.,* **19,** 371–380.

Chu, P. C., 1999: Two kinds of predictability in the Lorenz system. *J. Atmos. Sci.,* **56,** 1427–1432.

Dickinson, R. E., A. Henderson-Sellers, and P. J. Kennedy, 1993: Biosphere–Atmosphere Transfer Scheme (BATS) version 1e as coupled to the NCAR community climate model. NCAR Tech. Note NCAR/TN-387 + STR, 72 pp.

Faures, J. M., D. C. Goodrich, D. A. Woolhiser, and S. Sorooshian, 1995: Impact of small-scale spatial variability on runoff modeling. *J. Hydrol.,* **173,** 309–326.

Grell, G. A., J. Dudhia, and D. R. Stauffer, 1995: A description of the fifth-generation Penn State/NCAR mesoscale model (MM5). NCAR Tech. Note NCAR/TN-398 + STR, 122 pp.

Gupta, V. K., and E. Waymire, 1990: Multiscaling properties of spatial rainfall and river flow distributions. *J. Geophys. Res.,* **95,** 1999–2009.

Harris, D., and E. Foufoula-Georgiou, 2001: Subgrid variability and stochastic downscaling of modeled clouds: Effects on radiative transfer computations for rainfall retrieval. *J. Geophys. Res.,* in press.

——, M. Menabde, A. Seed, and G. Austin, 1996: Multifractal characterization of rain fields with a strong orographic influence. *J. Geophys. Res.,* **101** (D21), 26 405–26 414.

Kouwen, N., and G. Garland, 1989: Resolution considerations in using radar rainfall data for flood forecasting. *Can. J. Civ. Eng.,* **16,** 279–289.

Krajewski, W. F., L. Venkataraman, K. P. Georgakakos, and S. C. Jain, 1991: A Monte Carlo study of rainfall sampling effect on a distributed catchment model. *Water Resour. Res.,* **27,** 199–128.

Kumar, P., and E. Foufoula-Georgiou, 1993a: A multicomponent decomposition of spatial rainfall fields. 1. Segregation of large- and small-scale features using wavelet transforms. *Water Resour. Res.,* **29,** 2515–2532.

——, and ——, 1993b: A multicomponent decomposition of spatial rainfall fields. 2. Self-similarity in fluctuations. *Water Resour. Res.,* **29,** 2533–2544.

Lakhtakia, M. N., and T. T. Warner, 1994: A comparison of simple and complex treatments of surface hydrology and thermodynamics suitable for mesoscale and atmospheric models. *Mon. Wea. Rev.,* **122,** 880–896.

Li, Q., R. L. Bras, and S. Islam, 1995: Growth and decay of error in a numerical cloud model due to small initial perturbations and parameter changes. *J. Appl. Meteor.,* **34,** 1622–1632.

Michalakes, J., 1998: The same-source parallel MM5. *Proc. Second Int. Workshop on Software Engineering and Code Design in Parallel Meteorological and Oceanographic Applications,* Scottsdale, AZ, NASA GSFC Preprint CP-1998-206860, 129–139.

Michaud, J. D., and S. Sorooshian, 1994: Effect of rainfall-sampling errors on simulations of desert flash floods. *Water Resour. Res.,* **30,** 2765–2775.

Nykanen, D. K., 2000: Space-time variability of rainfall and soil moisture in coupled land–atmosphere modeling: Issues of scale and effect on predicted water and energy fluxes. Ph.D. thesis, University of Minnesota, Minneapolis, MN, 162 pp.

Obled, C., J. Wendling, and K. Beven, 1994: The sensitivity of hydrologic models, to spatial rainfall patterns: An evaluation using observed data. *J. Hydrol.,* **159,** 305–333.

Ogden, F. L., and P. Y. Julien, 1993: Runoff sensitivity to temporal and spatial rainfall variability at runoff plane and small basin scale. *Water Resour. Res.,* **29,** 2589–2597.

——, and ——, 1994: Runoff model sensitivity to radar rainfall resolution. *J. Hydrol.,* **158,** 1–18.

Perica, S., 1995: A model for multiscale disaggregation of spatial rainfall based on coupling meteorological and scaling descriptions. Ph.D. thesis, University of Minnesota, Minneapolis, MN, 145 pp.

——, and E. Foufoula-Georgiou, 1996a: Linkage of scaling and thermodynamic parameters of rainfall: Results from midlatitude mesoscale convective systems. *J. Geophys. Res.,* **101** (D3), 7431–7448.

——, and ——, 1996b: Model for multiscale disaggregation of spatial rainfall based on coupling meteorological and scaling descriptions. *J. Geophys. Res.,* **101** (D21), 26 347–26 361.

Porporato, A., P. D'Odorico, L. Ridolfi, and I. Rodriguez-Iturbe, 2000: A spatial model for soil–atmosphere interaction: Model con-

struction and linear stability analysis. *J. Hydrometeor.,* **1,** 61–74.

Schertzer, D., and S. Lovejoy, 1987: Physical modeling and analysis of rain and clouds by anisotropic scaling multiplicative processes. *J. Geophys. Res.,* **92** (D8), 9693–9714.

Siebert, J., U. Sievers, and W. Zdunkowski, 1992: A one-dimensional simulation of the interaction between land surface processes and the atmosphere. *Bound.-Layer Meteor.,* **59,** 1–34.

Stensrud, D. J., J. Bao, and T. T. Warner, 2000: Using initial condition and model physics perturbations in short-range ensemble simulations of mesoscale convective systems. *Mon. Wea. Rev.,* **128,** 2077–2107.

University Corporation for Atmospheric Research, 1992: General meteorological package (GEMPAK), version 5.1, reference manual. Unidata Program Center, Boulder, CO, 262 pp. [Available from University Corporation for Atmospheric Research. P.O. Box 3000, Boulder, CO 80307.]

Venugopal, V., E. Foufoula-Georgiou, and V. Sapozhnikov, 1999: A space–time downscaling model for rainfall. *J. Geophys. Res.—Atmos.,* **104** (D16), 19 705–19 721.

Wang, W., and N. L. Seaman, 1997: A comparison study of convective parameterization schemes in a mesoscale model. *Mon. Wea. Rev.,* **125,** 252–278.

Warner, T. T., R. A. Peterson, and R. E. Treadon, 1997: A tutorial on lateral boundary conditions as a basic and potentially serious limitation to regional numerical weather prediction. *Bull. Amer. Meteor. Soc.,* **78,** 2599–2617.

Winchell, M., H. V. Gupta, and S. Sorooshian, 1998: On the simulation of infiltration- and saturation-excess runoff using radar-based rainfall estimates: Effects of algorithm uncertainty and pixel aggregation. *Water Resour. Res.,* **34,** 2655–2670.

Yang, Z., and R. E. Dickinson, 1996: Description of the Biosphere–Atmosphere Transfer Scheme (BATS) for the Soil Moisture Workshop and evaluation of its performance. *Global Planet. Change,* **13,** 117–134.

Zhang, S., and E. Foufoula-Georgiou, 1997: Subgrid-scale rainfall variability and its effects on atmospheric and surface variable predictions. *J. Geophys. Res.,* **102** (D16), 19 559–19 573.